AAPS PharmSciTech, Vol. 9, No. 3, September 2008 (© 2008)
DOI: 10.1208/s12249-008-9134-9

Research Article

Importance of Small Pores in Microcrystalline Cellulose for Controlling Water Distribution during Extrusion–Spheronization

Josephine L. P. Soh,[1,2] Lei Yang,[3,4] Celine V. Liew,[5] Fu D. Cui,[3] and Paul W. S. Heng[5,6]

Received 4 April 2008; accepted 9 July 2008; published online 22 August 2008

Abstract. The purpose of this research was to investigate the effects of particle size on the wet massing behavior of microcrystalline cellulose (MCC). In this study, a series of six fractionated MCC grades were customized and specially classified to yield different particle size varieties of the standard grade, Comprecel M101. All seven MCC grades were extensively characterized for the physical properties and wet massing behavior using mixer torque rheometry. Effects of MCC physical properties on the maximum torque ($Torque_{max}$) were determined using partial least squares (PLS) analysis. Most physical properties varied systematically with particle size and morphological changes. Marked differences were observed in the small pore volumes (V_{highP}) and BET surface areas of the MCC grades. Variables that exerted dominant influences on $Torque_{max}$ were identified. In particular, the significance of V_{highP} in governing wet mass consistency was established. The role of V_{highP} has not been reported in any study because this small but significant variation is likely to be obliterated or compensated by variation in other physical properties from MCC grades from different suppliers. The findings demonstrated the role of small pores in governing the wet mass consistency of MCC and provide a better understanding of MCC's superior performance as a spheronization aid by the ability to fulfill the function as a molecular sponge to facilitate pellet formation during wet granulation processes.

KEY WORDS: extrusion–spheronization; microcrystalline cellulose; spheronization aid; torque rheometry.

INTRODUCTION

Microcrystalline cellulose (MCC) was initially developed and marketed as a directly compressible excipient for tableting. However, it is the utility of MCC in wet granulation, particularly in spheroid production, that generated considerable research interest in the past few decades. The motivation that drives forth these activities was largely because the unparalleled efficiency of MCC as a spheronization aid has not been affirmatively proven. MCC has widely been described as a "molecular sponge" due to the ability to retain a large amount of water yet allowing this stored water to be released or evaporated with great ease (1). This feature is believed to be crucial in the precise control of water movement or distribution within wetted powder masses that are to be subsequently extruded and spheronized. Still, the "sponge model" was not able to explain the failure of other materials to function as well as MCC despite having the ability to hydrate and absorb considerable amounts of water. Subsequently, a crystallite-gel model (2) was proposed in an attempt to provide an alternative explanation for MCC's mechanism of action in spheroid formation.

From the encouraging performance of crospovidone to aid in extrusion–spheronization, Liew *et al*. (3) concluded that for any given material to serve as a competent spheronization aid, the internal water repository has to possess adequate capacity and rigidity to modulate the amount of water released under pressure for lubrication during extrusion. While many previously proposed materials have the ability to absorb water, these materials lacked the rigidity and binding ability (of MCC) to regulate water distribution by coping with the pressures exerted during extrusion–spheronization. To date, a clear explanation of the mechanism by which MCC acts as a rigid molecular sponge-like structure has not been affirmatively agreed or answered though it is widely believed to lie within the pore structure of MCC.

The main hypothesis of this work was that the internal water repository of MCC or any potential alternative to MCC must be made up of both large (>10 μm in diameter) and small pores (<10 μm in diameter) in order for it to function effectively as a spheronization aid. In fact, it is the network of small pores that provides the so-called rigidity to the molecular sponge because water trapped in the small pores

[1] Department of Industrial and Physical Pharmacy, School of Pharmacy and Pharmaceutical Sciences, Purdue University, 575 Stadium Mall Drive, West Lafayette, Indiana 47907, USA.
[2] *Present address:* Pfizer Global Research and Development, Sandwich Laboratories, Kent, UK.
[3] School of Pharmacy, Shenyang Pharmaceutical University, Shenyang, 103 Wenhua Road, 110016, China.
[4] *Present address:* GlaxoSmithKline Research and Development Centre, Tianjin, China.
[5] Department of Pharmacy, National University of Singapore, 18 Science Drive 4, S117543, Singapore, Singapore.
[6] To whom correspondence should be addressed. (e-mail: phapaulh@nus.edu.sg)

is less readily released unless considerable stresses are exerted, e.g. during extrusion and spheronization. Thus, the sub-hypothesis was that water stored within the small pores served as a secondary reservoir to release that small but critical amount of moisture for lubrication and plasticization of the moistened mass into spherical granules or spheroids. As long as a material possesses both small and large pores, in addition to previously listed criteria (3) such as low water solubility and good binding abilities, it is very likely to be able to function as an effective spheronization aid.

In earlier studies, it was identified that V_{lowP} (which denoted the volume of pores whose diameters are larger than 10 μm) and density of MCC were the main characteristics governing the performance of MCC in extrusion–spheronization (4,5). These findings were consistent with the behavior of MCC as a molecular sponge and lent support to the proposed hypothesis of this present study. Yet, there has been no study reported to date that can prove the critical role of small pores (herein defined as pores which are lesser than 10 μm in diameter and denoted as V_{highP}) in controlling water distribution during wet massing and spheroid production.

One of the plausible reasons was that most studies were either conducted with a small number of MCC grades or that the MCC grades used were obtained from different suppliers. The effect of source variation on MCC's physical properties and performance in pharmaceutical applications was well documented (4–10) and very likely to confound the true effects and contributions of each property. In fact, MCC grades from different manufacturers have been found to have similar wet massing behavior (5) and possibly comparable extrusion–spheronization performance (6) because the unique set of physical properties could have interacted in a way to cancel out or compensate for the differences. Expectedly, this masking effect will be more pronounced for those physical attributes that do not exhibit marked or systematic variations between MCC grades which make them readily overlooked in correlation analysis.

With these considerations in mind, it was essential to use MCC grades that were not only from the same manufactured batch but differ systematically in certain fundamental properties such as particle size. This could be likened to amassing a homologous series of MCC grades which, unlike other synthetic polymers was not as straightforward due to the inherent variabilities associated with the starting material (wood pulp) used for MCC production. Hence, six MCC grades were specially produced by the manufacturer for this study using the same pulp material and fractionated to yield different particle sizes. The first step to test the proposed hypothesis was to identify the critical variables that affect the torque rheological properties of wet MCC masses. These in turn, had been previously shown to be able to predict the quality of spheroids prepared by extrusion–spheronization (5,6).

Therefore, it was believed that the importance of small pores (V_{highP}) in controlling the wet massing behavior of MCC and in turn, the extrusion–spheronization performance could be proven in a similar way using a specially manufactured homologous series of MCC grades. This knowledge could then contribute another dimension to the elucidation of MCC's unique functionality and efficiency as a spheronization aid.

MATERIALS AND METHODS

Materials

Six particle size variants of a standard MCC grade (Comprecel M101, Mingtai Chemical, Taiwan, Republic of China) were custom-produced by the manufacturer (Mingtai Chemical, Taiwan, Republic of China) for this study and were prepared by size fractionation. These six batches will be referred to as MCC-A, MCC-B, MCC-C, MCC-D, MCC-E and MCC-F, in descending order of particle sizes. M101 was included in this study as a control.

Methods

Physical Characterization of Various MCCs

Particle Size and Size Distribution. All powders were pre-sieved with a 1 mm aperture size sieve before size analysis by laser diffraction (Dry Powder Module, LS230, Coulter Corporation, USA). Powders were steadily delivered to achieve an obscuration of 4–7%. Sampling time was fixed at 60 s. Volume weighted mean particle size (X_{50}) was automatically determined while particle size distribution was represented by span and calculated as follows.

$$\text{Span} = \frac{X_{90} - X_{10}}{X_{50}} \quad (1)$$

where X_{10}, X_{50} and X_{90} were the diameters of powder particles at the 10, 50 and 90 percentiles of the cumulative percent undersize plot respectively. Five repeats were carried out.

Particle Morphology Using Scanning Electron Microscopy (SEM). Powder samples were mounted on studs using double-sided carbon tape and gold coated. Photomicrographs of the samples were obtained using a scanning electron microscope (JSM-5200, Jeol Ltd, Japan) under different magnifications.

Crystallinity. X-ray diffractograms of the MCC powders (n=4) were measured using an X-ray diffractometer (XRD 6000, Shimadzu, Japan). A monochromatic CuKα radiation source was operated at 40 kV and 30 mA with a scanning rate of 1° (2θ)/min over a range of 5–45° (2θ). Percent crystallinity was assessed on the basis of a two-phase concept used by Hermans and Weidinger (11) and calculated according to the equation below.

$$X_{cr} = \frac{I_{cr}}{I_{cr} + I_a} \quad (2)$$

where I_{cr} and I_a were the crystalline and amorphous peak intensities, respectively.

Micromeritic Properties. Micromeritic properties of the MCC powders (n=3) were evaluated using mercury intrusion porosimetry (Model 9320, Micromeritics, USA). The contact angle, surface tension and density of mercury were taken as 130°, 485 dyne/cm (0.485 N/m) and 13.53 g/ml respectively.

The bulb of a 5 ml penetrometer was filled with powder and subjected to gradual vacuum evacuation. Mercury filled the penetrometer bulb at an initial pressure of 0 MPa. As the pressure increased from 0 to 0.172 MPa, mercury began to intrude pores that ranged between 250 to 10 μm. Higher pressures (0.172–207 MPa) were required to fill the smaller pores present (10–0.006 μm). V_{lowP} and V_{highP} referred to the specific cumulative intruded mercury volume into the pores as the pressure was increased from 0 to 0.172 MPa and 0.172 to 207 MPa, respectively. The total specific intrusion volume for each sample within the entire pressure range of 0–207 MPa was denoted as V_{total} and calculated as a sum of V_{lowP} and V_{highP}. V_{total} represented the total pore volume per unit weight of sample and was used in the calculation of percent porosity (ε) where

$$\varepsilon = \left(1 - \frac{\rho_e}{\rho_a}\right) \times 100\%. \quad (3)$$

Bulk density of sample, ρ_e was $\frac{W_{sample}}{V_{penetrometer} - V_{Hg}}$, absolute density of sample, ρ_a was $\frac{W_{sample}}{(V_{penetrometer} - V_{Hg}) - V_{total}}$, W_{sample} was the sample weight, $V_{penetrometer}$ was the volume of the empty penetrometer and V_{Hg} was the volume of mercury filled into the penetrometer at 0 MPa.

Powder Densities. True densities of all the MCC size types were estimated using a helium pycnometer (Penta-Pycnometer, Quantachrome Instruments, USA). The MCC powders were pre-dried in a convection oven at 105°C and cooled under vacuum in a dessicator before use. Large sample cells were filled to 90% with the dry MCC powders and purged with helium gas for 10 min before actual analysis commenced. Analysis was performed in triplicates and results averaged.

Bulk (ρ_b) and tapped (ρ_t) densities were calculated as the quotients of the weight of filled powder in the cylinder and the volume occupied by the powder before and after tapping, respectively (n=3). Tapping was conducted on a tapping apparatus (Stampfvolumeter, JEL, Germany) and performed in a 2^n geometric progression until no change in volume. MCC powders were equilibrated at 25°C, 50% relative humidity (RH) for 72 h prior to use. Carr indices and Hausner ratios were subsequently derived as shown in the following equations (12,13).

$$\text{Carr index} = \frac{\rho_t - \rho_b}{\rho_t} \quad (4)$$

$$\text{Hausner ratio} = \frac{\rho_t}{\rho_b}. \quad (5)$$

Flow Properties. Repose angles and angles of fall (n=3) were measured using a powder tester (Powder Tester, Hosokawa Micron, Japan) using 35 g of powder that flowed through the glass funnel onto a 710 μm aperture size sieve vibrated at an amplitude of 1 mm. The sieved powder was directed from another glass funnel to form a heap on the stainless steel stand positioned underneath it. The angle formed between the side of the heap and the horizontal is defined as the repose angle, α_r. Three mechanical shocks were applied to the stationary powder mass which caused it to collapse. The new angle formed between the side of the new heap and the horizontal is the angle of fall, α_f. The difference between the angles of repose and fall is the angle of difference, α_d.

Avalanche flow properties of MCC powders were tested using a powder flowability analyzer (Aero-Flow™, Model 3250, TSI Incorporated, USA). MCC powders were oven-dried at 105°C for 4 h and equilibrated in ambient conditions (25°C, 50% RH) for 72 h prior to use. Equilibrated powders amounting to a volume of 60 cm^3 was placed in the sample drum and tested at seven different drum speeds from 60–240 s/rev. Ease of powder flow can be represented graphically in the form of strange attractor plots and quantified using two proposed indices (14), avalanche flow index (AFI) and cohesive interaction index (CoI).

$$\text{AFI} = 1/m \quad (6)$$

where m is the gradient of the graph for mean time to avalanche (MTA) against drum speed. A larger AFI value is indicative of better flow.

$$\text{CoI} = n \quad (7)$$

where n is the gradient of the graph for scatter against drum speed. A larger CoI value is indicative of higher cohesiveness.

Specific Surface Area. Specific surface areas (SSA) of the MCC grades (n=3) were determined using the multi-point BET adsorption method (SA3100, Coulter, USA) using nitrogen as the adsorbate gas. The powder samples were degassed for 16 h under nitrogen at 70°C to remove any pre-adsorbed gases and vapors from the powder surface. Multi-point measurements were made in the partial pressure range of 0 to 0.3.

Wet Massing Studies Using Torque Rheometry

Wet massing behavior of MCCs was determined in the same way as reported in the earlier studies (6). Fifteen grams of MCC powder were added into the mixer bowl of the mixer torque rheometer—MTR (Caleva Process Solutions, England) and mixed for 30 s. The mean torque generated by the dry powder was recorded. Distilled water, corresponding to water addition aliquots of 15% *w*/*w* was added to the dry powder at intervals of 30 s for the first ten additions and at intervals of 60 s for the remaining nine additions. The entire mixing process was completed in 20 min and mean torques generated for 19 additions were recorded. The water content range investigated spanned from 0 to 285% *w*/*w*.

Extrusion–Spheronization Parameters

A 30 g powder blend of MCC/lactose monohydrate (Pharmatose 200M, DMV International, The Netherlands) in the ratio of 3:7 was wet massed with 20–45% *w*/*w* water (4). The wetted mass was manually extruded through a 1 mm aperture size mesh and spheronized in a small scale spheronizer (Model 120, Caleva Process Solutions, UK) fitted with a friction plate of 12 cm diameter at 1,500 rpm for 5 min. The plate had a cross-hatch pattern with studs that were 1.2 mm

wide and 2 mm apart. Spheroids produced were oven-dried (60°C, 4 h), sieved through a nest of sieves of aperture sizes in a $\sqrt{2}$ progression from 250–2,800 μm on a mechanical sieve shaker (VS 1000, Retsch, Germany) for 10 min at an amplitude of 1 mm.

$W_{710\ \mu m}$ referred to the percentage of water content required to produce spheroids of 710 μm and was determined from the linear plot of log d_{geo} (Eq. 8) against the amount of water used. W_s denoted the spheronization water sensitivity of a given MCC grade and was the gradient of the same plot.

$$\log d_{eeo} = \frac{\sum(W_i \times \log d_i)}{\sum W_i}. \quad (8)$$

Statistical Analysis

Partial least squares (PLS) analysis was performed using a multivariate analysis software (SIMCA P+, Umetrics Academy, Sweden). All variables were scaled to unit variance. Analysis of variance (ANOVA) and Pearson's correlation analysis were performed using statistical software (SPSS Version 13.0 for Windows, SPSS, USA).

RESULTS AND DISCUSSION

Powder Properties

Particle Size and Morphology

Table I shows the physical properties of the MCC types, in decreasing chronological order of particle sizes from 255.45 μm (MCC-A) to 36.64 μm (MCC-F). The standard grade, M101 had a mean particle size of 65.37 μm. Particle size distributions of the MCC types, denoted by the span values (Table I) increased as mean particle sizes were reduced which indicated greater heterogeneity in particle sizes within the bulk powder masses of smaller MCC grades (MCCs E–F and M101). Clear differences in particle morphologies were observed between the different size types (Fig. 1). Larger MCC types (MCCs A–C) were composed of agglomerated particles while MCCs E–F and M101 were almost exclusively made up of discrete individual particles that were needle-shaped. It could also be seen that as particle sizes decreased, the shape of the MCC particles changed from generally round (Fig. 1a, b) to long, needle-shape fibers as seen in the remaining electron micrographs.

Table I. Physical Properties of MCC Grades

	MCC-A	MCC-B	MCC-C	MCC-D	MCC-E	Comprecel M101	MCC-F
Particle size (μm)	255.45	188.50	153.45	109.30	74.97	65.37	36.64
	(0.64)	(1.13)	(0.07)	(0.00)	(0.95)	(0.00)	(0.80)
Span	0.85	0.97	1.12	1.30	1.55	1.59	1.65
	(0.00)	(0.01)	(0.01)	(0.00)	(0.03)	(0.01)	(0.04)
X_{cr} (%)	56.77	57.73	59.44	61.57	66.86	62.26	64.54
	(2.23)	(1.01)	(3.19)	(1.39)	(1.94)	(0.38)	(0.76)
ε (%)	66.34	63.21	62.45	57.98	67.58	67.39	64.99
	(2.97)	(2.36)	(0.86)	(1.11)	(1.56)	(1.78)	(1.30)
SSA (m^2/g)	1.000	1.005	1.023	0.956	0.849	1.173	1.098
	(0.006)	(0.011)	(0.006)	(0.024)	(0.066)	(0.038)	(0.04)
True density (g/ml)	1.55	1.55	1.55	1.55	1.55	1.55	1.55
	(0.01)	(0.00)	(0.01)	(0.01)	(0.02)	(0.00)	(0.01)
Bulk density (g/ml)	0.24	0.26	0.26	0.28	0.30	0.31	0.35
	(0.002)	(0.003)	(0.003)	(0.002)	(0.003)	(0.01)	(0.014)
Tapped density (g/ml)	0.32	0.37	0.39	0.41	0.44	0.50	0.52
	(0.003)	(0.002)	(0.005)	(0.006)	(0.014)	(0.01)	(0.01)
Carr index (%)	27.0	30.0	31.7	31.7	32.0	37.7	33.7
	(0.01)	(0.01)	(0.01)	(0.01)	(0.02)	(0.02)	(0.02)
Hausner ratio	1.37	1.43	1.46	1.46	1.47	1.61	1.51
	(0.02)	(0.02)	(0.03)	(0.01)	(0.04)	(0.04)	(0.03)
σ_r (°)	43.5	43.9	46.0	47.7	50.9	52.0	54.0
	(0.1)	(0.6)	(0.5)	(0.5)	(0.8)	(1.1)	(0.2)
σ_f (°)	27.6	25.6	26.7	26.8	28.1	30.4	28.7
	(0.8)	(1.0)	(0.3)	(1.3)	(0.4)	(0.8)	(0.8)
σ_d (°)	16.3	17.9	19.3	20.8	22.8	21.7	25.2
	(0.8)	(1.6)	(0.3)	(0.8)	(0.5)	(1.1)	(0.8)
$W_{710\ \mu m}$ (% *w/w*)	43.67	43.79	43.82	43.60	44.00	42.64	42.72
	(0.07)	(0.04)	(0.04)	(0.01)	(0.03)	(0.17)	(0.27)
W_s	6.22	6.18	6.32	6.35	6.36	5.10	6.54
	(0.40)	(0.20)	(0.17)	(0.19)	(0.23)	(0.24)	(0.14)

Values in parentheses represent the standard deviations.
X_{cr} percent crystallinity, ε porosity, σ_r, σ_f and σ_d angles of repose, fall and difference, respectively, *SSA* specific surface area, $W_{710\ \mu m}$ water content needed to prepare spheroids that are 710 μm in diameter, W_s water sensitivity

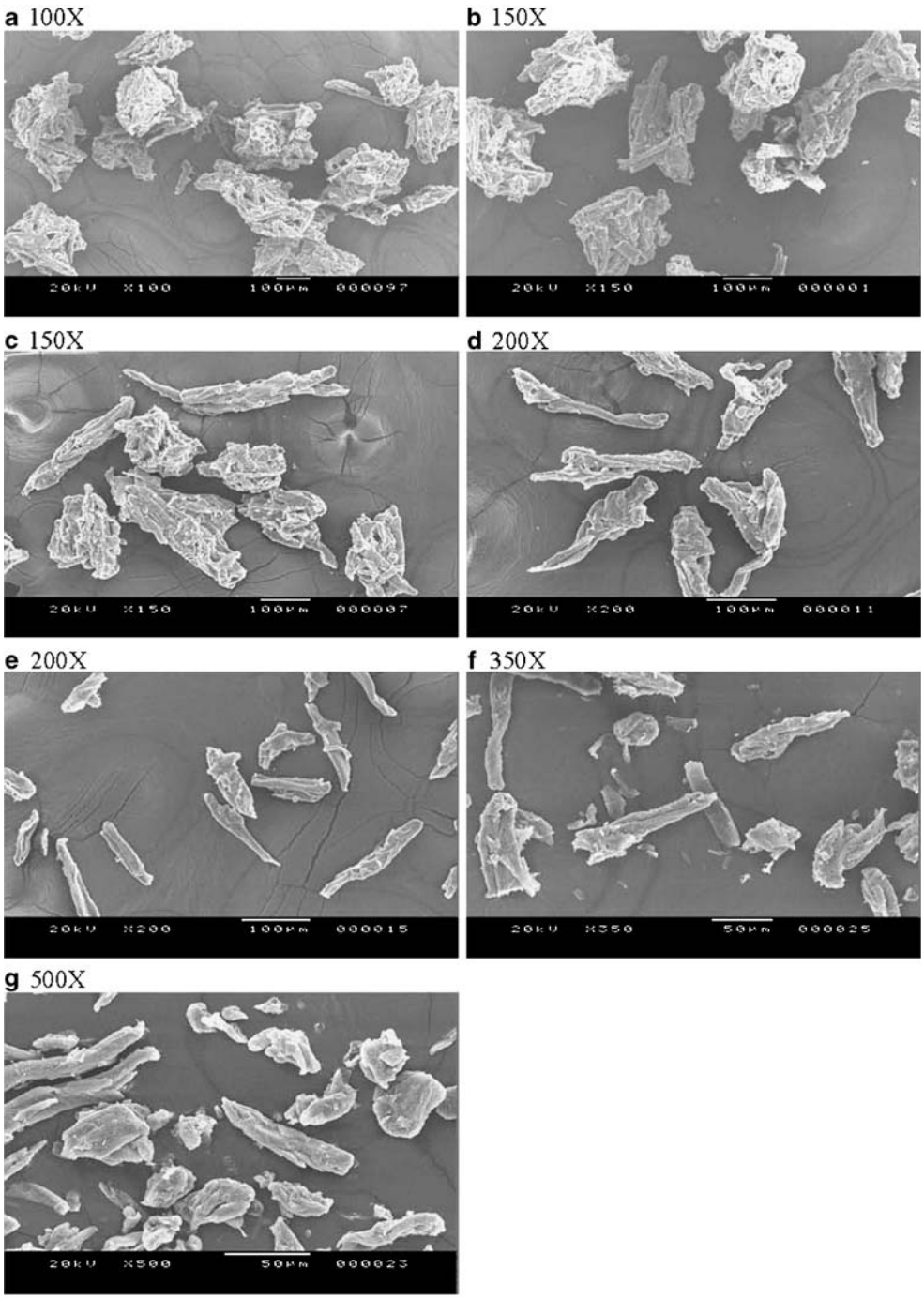

Fig. 1. Scanning electron micrographs of **a** MCC-A, **b** MCC-B, **c** MCC-C, **d** MCC-D, **e** MCC-E, **f** Comprecel M101 and **g** MCC-F

X-Ray Diffraction and Crystallinity

Crystallinities of the various MCC types were significantly different (ANOVA, $p<0.05$) and tabulated in Table I. The respective X-ray diffractograms are shown in Fig. 2. Crystalline peaks were observed at 15°, 16° and 22° (2θ) which were characteristic of cellulose I, the native cellulose type. Additionally, a distinct shoulder was also found at 20° (2θ) on all the diffractograms which indicated the presence of cellulose II which was the solubilized and regenerated or chemically swollen and recrystallized cellulose I (9). MCC grades that possessed cellulose II were believed to have undergone more rigorous manufacturing conditions (9) though this was also dependent on the source or type of wood pulp used for the MCC manufacture. Regardless of particle size, the seven MCCs employed in this study were found to contain Cellulose II suggesting that these MCCs were produced using the same type of wood pulp or starting material under the same manufacturing conditions. This is of particular significance in this study because it meant that particle size effects of MCC can be elucidated without the confounding influence of source variation.

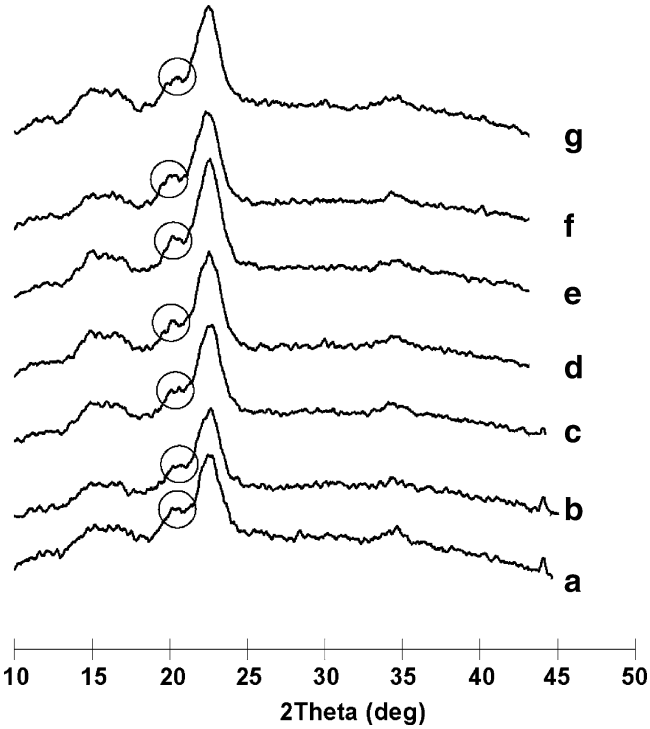

Fig. 2. X-ray diffractograms of MCC powders. **a** MCC-A, **b** MCC-B, **c** MCC-C, **d** MCC-D, **e** MCC-E, **f** Comprecel M101 and **g** MCC-F. Additional shoulders at 20° (*circled*) indicated presence of cellulose II

Micromeritic Properties

A noteworthy trend was observed between the pore volumes, V_{lowP} and V_{highP} and MCC particle size and size distribution. Micromeritic properties of the seven MCC grades could be broadly divided into group 1 (MCCs A–C) and group 2 (MCCs D–F and M101). For group 1, V_{lowP} values increased as the MCC particle size decreased (Fig. 3) which meant that the volume of mercury intruded into pores larger than 10 μm was correspondingly larger for MCC-C compared to MCC-B and MCC-A. On the contrary, V_{highP} values decreased within this group of MCCs. Further reduction in MCC particle size from MCC-D to MCC-F (Group 2) led to a reversal in this trend where V_{lowP} values decreased while V_{highP} values increased.

The increase in V_{lowP} values from MCC-A to MCC-C was plausibly attributed to the change in shape of MCC particles from roundish agglomerates in MCC-A to progressively elongated agglomerates in MCCs B and C (Fig. 1a–c). In general, particles that are more spherical tend to pack better and more closely as compared to elongated particles (especially those with jagged edges) which are more likely to interlock and stack on top of each other. This form of particle arrangement creates considerable gaps between particles. As V_{lowP} is determined from low pressure mercury intrusion and reflects the relative magnitude of inter-particulate pore volumes, it is very much a function of powder packing. Consequently, the rise in V_{lowP} values from MCC-A to MCC-C was not unexpected. The remaining MCCs were almost exclusively composed of individual needle-shaped fibers (Fig. 1d–g) whose powder packing abilities were largely enhanced by the considerably wide particle size distributions which in turn, led to the observed decrease in V_{lowP} values.

On the other hand, V_{highP} denotes the volume of mercury intruded into small, intra-particulate pores (<10 μm). From Fig. 1a, it was clear that each particle of MCC-A was composed of many randomly orientated needle-shaped fibers bound together randomly during the spray drying stage of manufacture. This random packing of MCC fibers into a single MCC particle creates tiny voids within the particle which could have explained the large V_{highP} value for MCC-A. For MCCs B and C, the fibers were mostly aligned in the same general direction by binding side to side which led to the overall elongated shape and also minimized intra-particulate spaces (small V_{highP} values).

For the even smaller MCCs (MCC-E, M101 and MCC-F) that existed as single, discrete fibers, small fragments were also found to be present on the electron micrographs of M101 and MCC-F (Fig. 1f, g). These fractions of MCC fibers were believed to be fragments or comminuted particles. Small particles were also more cohesive in nature and when agitated, self-assembled into small agglomerates. Comminuted particles were also likely to contain fractures, crevices and surface impairments. Collectively, when the MCC fibers from the smaller size fractions were mercury intruded under high pressure, the self-assembled agglomerates and fractured fragments could have contributed to the large V_{highP} values for small MCC particle sizes, especially M101 and MCC-F. The correspondingly large BET surface areas for M101 and MCC-F (Table I) strongly supported the respective large V_{highP} values observed. Similarly, MCC-E which clearly appeared as smooth fibers under the SEM (Fig. 1e) was found to have the lowest BET surface area.

Powder Densities and Compressibility

Generally, true densities of the various MCC grades were similar though bulk and tapped densities were found to increase with decreasing particle size and shape changes from relatively spherical particles to discrete needle-shaped ones (Table I and Fig. 1). Small particles that were also more

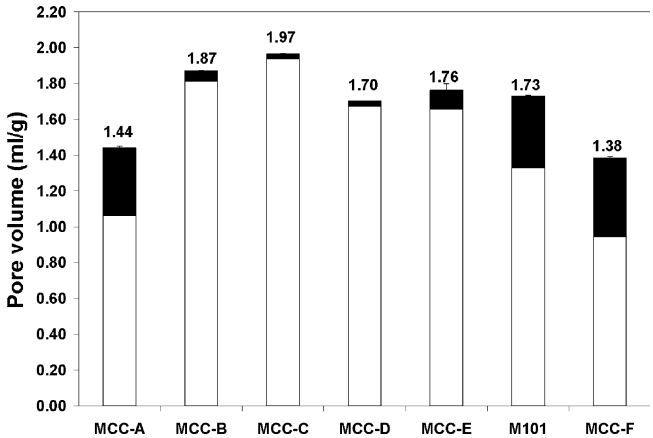

Fig. 3. Pore volumes of pores larger than 10 μm denoted by V_{lowP} (*unshaded*) and smaller than 10 μm denoted by V_{highP} (*shaded*) columns. Total pore volumes (V_{total}) were shown above the respective columns. $V_{total}=V_{lowP}+V_{highP}$

heterogeneous in size (as reflected by larger span values) could achieve closer packing. This was shown in the correlation results between particle size and bulk and tapped densities ($r^2 = -0.947$, $p = 0.001$; $r^2 = -0.957$, $p = 0.001$ respectively). Surface protuberances found in MCCs A–C hinder close packing of particles and result in particles being stacked on top of one another, trapping considerable volumes of air in between. Furthermore, the larger particle sizes and greater size homogeneity meant that there would always be inter-particulate gaps that could only be filled by much smaller particles. Thus, bulk and tapped densities of larger MCCs were low.

Both Carr indices and Hausner ratios increased as particle size decreased, indicating that powder packing property or compressibility worsened with smaller particles. However, it should be reminded that both Carr indices and Hausner ratios were largely dictated by the ratio and difference between bulk and tapped densities. Powders that have large differences between bulk and tapped densities tend to have larger Carr index and Hausner ratio values. For the larger MCCs, small differences between the bulk and tapped densities arose because the tapping process would not improve powder packing further as there were limited amount of small particles to fill the gaps for these fractionated particles. Thus, the significance of Carr index and Hausner ratio in defining the propensity of powders to be compressed should not be simply interpreted on the basis of the values obtained.

Flow Properties

Smaller particle size MCC powders had poorer flow and were more floodable (higher α_r, α_f, α_d) than the larger MCC particles as shown from the greater angle of difference, α_d (ANOVA, $p<0.05$). Under Carr's classification system (12), all these MCCs were considered as floodable with passable (MCCs-A and -B) and poor (MCCs-C-F and M101) flow.

Another method of flow characterization is based on powder avalanches. Although a comparatively newer flow measurement method, it can be considered as a more dynamic method since flowability is evaluated while the powder mass is in motion (rotating in the drum). Avalanche flow properties are evaluated qualitatively by comparing the strange attractor plots (Fig. 4). Larger MCC grades were characterized by dense plots (centers close to origin), indicating that the MTAs were shorter. Small particle size MCCs took much longer times to avalanche and there was much more variability between the times to avalanche, as denoted by the wider spread of points (scatter) on the plot.

From the AFI and CoI values (Fig. 5), avalanche flow properties of the MCCs were largely concordant with results from angles of repose and compressibility indices (Table I). However, it was interesting to note the unusually low AFI value of MCC-A which had been shown to possess the best flow properties in the other tests. In fact, it could also be seen in the strange attractor plot for MCC-A that the center of the plot was further from the origin than for MCC-B even though it had a much narrower spread of points (Fig. 4). This meant that MCC-A's MTA was longer than MCC-B's despite a lower cohesiveness between the particles.

Ease of powder avalanches can also be influenced by density and the type of flow motion during avalanching as reported by Lee *et al.* (18). To investigate the flow motion for the MCCs, a separate run was conducted for each MCC with the door of the cabinet housing the AeroFlow^{TM} tester open to enable visual observations of the flow pattern during avalanching. A drum speed of 120 s/rev was chosen because the drum speed used should neither be too fast nor too slow and this was the median of the seven drum speeds tested.

Four types of flow motion could be used to describe powder avalanches: "rolling", "slumping", "slipping" and "cataracting" in descending order of good flowability (18). MCC-A was found to exhibit a mixture of slumping and slipping during avalanches while MCC-B was often seen to slump in portions. This meant that the powder mass was avalanching like two portions of powder, one after another, instead of avalanching as a single homogenous mass. Consequently, the MTA of MCC-B was shorter than that of MCC-A which led to the higher AFI value for MCC-B.

Similar observations were found for the other MCCs. However, as cohesiveness was higher (higher CoI) due to smaller particle sizes, the corresponding MTA values were higher (lower AFI values). Furthermore from MCC-D onwards, cataracting became more prevalent within the avalanching powder mass. In particular, MCC-F could also be seen to cataract as a single cohesive mass which corroborated with the high CoI value (Fig. 5). Evidently, a comprehensive evaluation of avalanche flow behavior requires both quantitative (AFI and CoI) and qualitative (visual) observations.

Wet Massing Behavior Determined Using Mixer Torque Rheometry

All MCCs displayed distinctive torque profiles concordant with the various stages of liquid saturation (Fig. 6). Despite the marked difference in particle sizes, the seven MCCs investigated in this work were shown to have the same $\%H_2O_{(maxT)}$ value at 135% *w/w*. This meant that the water contents required to achieve respective maximum torques were similar. These results contradicted the report by Rowe and Sadeghnejad (19) which concluded that a reduction in particle size would lead to lower water requirements for achieving saturation (maximum torque).

The magnitudes of maximum torque achieved were almost identical for MCCs-A to MCC-D (ANOVA, $p>0.05$). Beyond 90% *w/w* water, the torque responses achieved by MCC-E were consistently lower than the other MCCs' (ANOVA, $p<0.05$) and this was believed to result from the intrinsic morphological characteristics of MCC-E. MCC-E particles were seen to be exceptionally smoother than all the other MCCs (Fig. 1), with minimal surface defects or fractures for imbibing water during wet massing. As a result, a larger portion of the added water was available in the inter-particulate spaces to lubricate the mixing process, leading to lower torque values. On the other hand, the wet mass consistency of M101 and MCC-F started to rise much more than the other five MCCs after 75% *w/w* of water was added (Fig. 6).

Effects of MCC physical properties on $Torque_{max}$ was clearly demonstrated in the PLS plots (Fig. 7). The W_{710} value had a strong negative correlation with $Torque_{max}$ while SSA had a strong positive correlation (Fig. 7a). This meant that

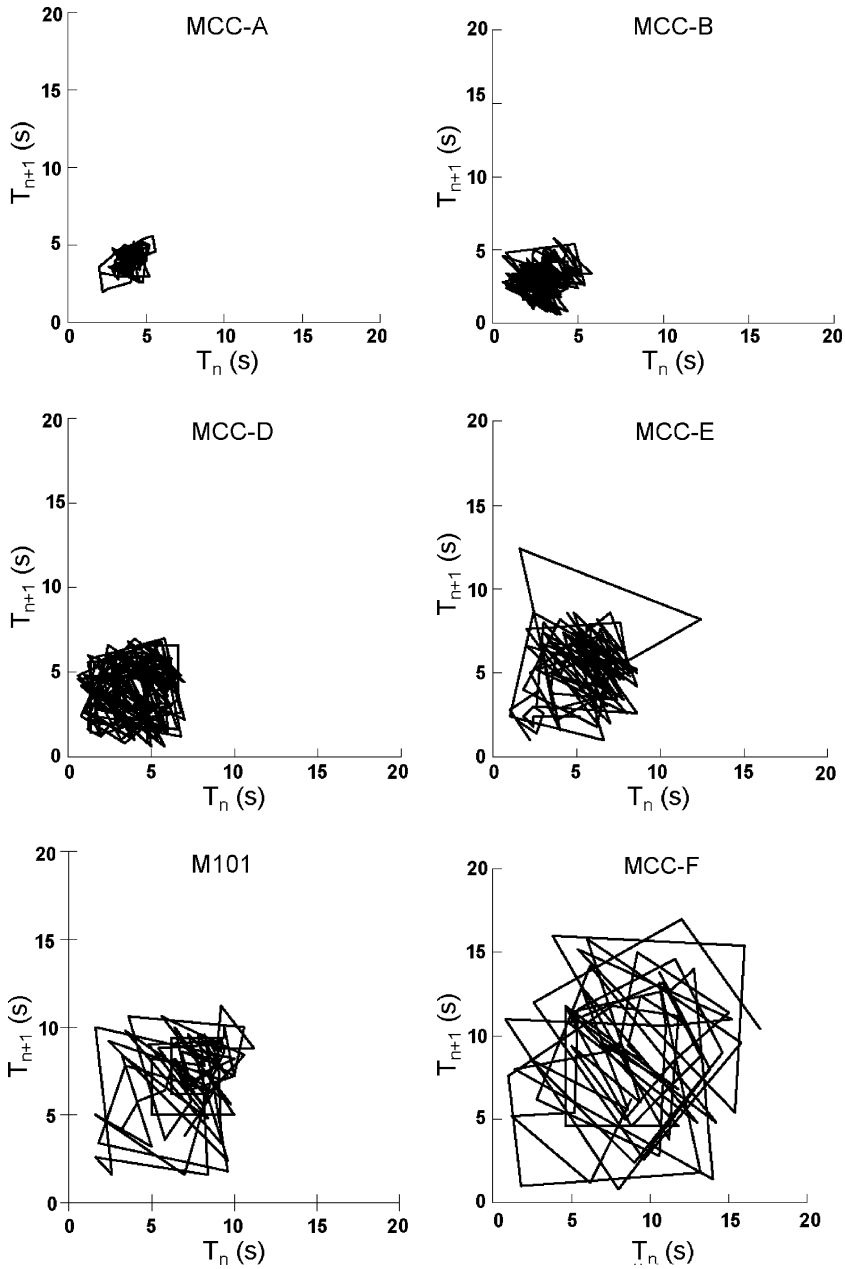

Fig. 4. Strange attractor plots for MCC grades

MCC grades with a larger $W_{710\ \mu m}$ value and smaller SSA tend to generate a smaller $Torque_{max}$. The relationship between packing abilities of MCC powders (bulk and tapped densities) and wet mass consistency has been well established and explained (3–6). Variables which had very large error bars (confidence intervals) spanning the positive and negative regions were not deemed to have significant effects.

When the less significant variables were excluded from modeling $Torque_{max}$, a one component model with a strong goodness of fit (R^2X=0.732) and strong model predictability (Q^2cum=0.973) was achieved. In general, a Q^2cum value (cross validation) greater than 0.5 indicated good model predictability (20). A good fit was also found between the observed *versus* predicted values of $Torque_{max}$, in this model. What was more interesting was the relationship established between V_{highP} and $Torque_{max}$ as shown in both multivariate (Fig. 7) and univariate correlation (r^2=0.757, p= 0.048). MCC grades with larger V_{highP} value tended to yield a corresponding larger $Torque_{max}$. However, MCC-A appeared to be an aberration to this rule since the $Torque_{max}$ value was not as high as those of MCC-F and M101 despite a similar V_{highP} value. This could possibly be attributed to two reasons. Firstly, the SSA value of MCC-A was approximately 10–18% lower than that of the other two MCCs. This suggested that the water absorption into the particles and for binding between particles were impaired or less efficient which in turn affected the $Torque_{max}$ value which reflects the resistance exerted by the wetted mass onto the mixer blades. The major reason, is more likely to be that of the marked difference in bulk and tapped densities where MCC-A was almost 1.5 times less dense than for the latter two MCCs. It is obvious that a denser powder and subsequently,

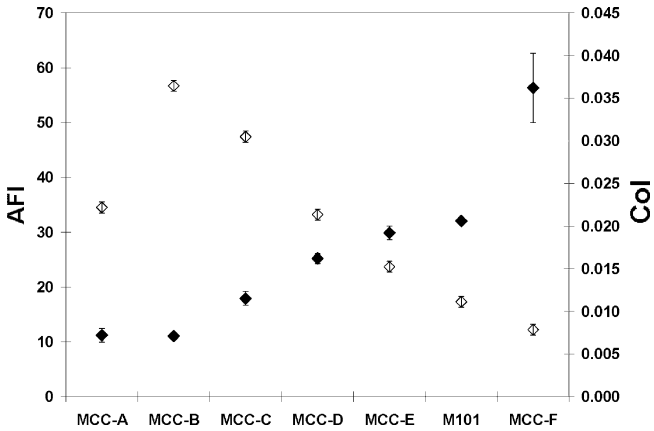

Fig. 5. Avalanche flow index (*AFI*) and cohesive interaction index (*CoI*) of MCC grades

wetted mass provides more resistance to the mixing process and in turn leads to higher $Torque_{max}$ values for M101 and MCC-F.

Another possible issue of contention is the apparent disagreement between the $Torque_{max}$, $W_{710\ \mu m}$ and W_s values (Table I). While the $W_{710\ \mu m}$ and W_s values can be regarded as more direct indicators of water sensitivity and wet massing behavior, it must also be noted that the variability that is involved in the determination is also considerably higher than that for $Torque_{max}$. These included: the amount of water accurately sprayed onto the powder mass during wet massing and the goodness of fit between the various points of the plot of log d_{geo} *vs.* the amount of water. In particular, a slight shift in any particular point can lead to considerable changes in the $W_{710\ \mu m}$ and W_s values even though care has been taken to ensure that the experiments were at least performed in triplicates. On the other hand, $Torque_{max}$ determination only involved dosing of the granulating water through a syringe which is comparatively more accurate. Despite this, the significant negative correlation between $Torque_{max}$ and $W_{710\ \mu m}$ values was still shown in multivariate analysis (Fig. 7b).

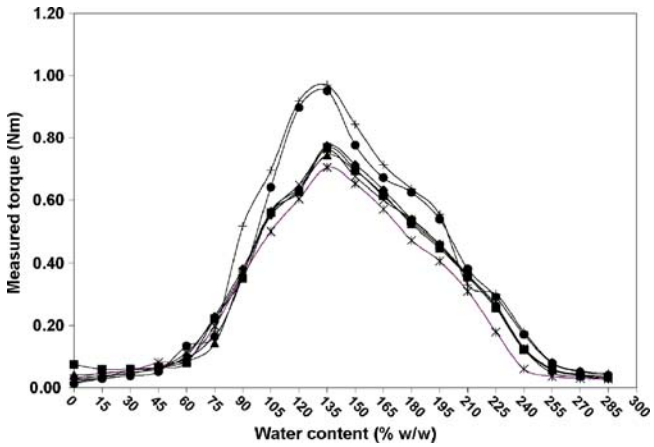

Fig. 6. Variation of measured torque (Nm) with increasing water content for (♦) MCC-A, (■) MCC-B, (▲) MCC-C, (×) MCC-D, (*) MCC-E, (+) Comprecel M101 and (●) MCC-F

The influence of V_{highP} on many aspects of MCC's behavior in torque rheometry and extrusion–spheronization has always been minor in previous studies (4–6). Instead, the control of water movement in and out of the pores and the unique functionality of MCC as a molecular sponge were often deemed to be dominated by V_{lowP} and V_{total} which represented the volumes (capacity) of the large pores (>10 μm) within the MCC particles. Especially when MCC grades sourced from different suppliers were compared, variabilities in physical properties could have also obliterated the small but significant role of V_{highP} in the control of water distribution.

This was by far the first study that demonstrated a possible role of small pores in contributing to the utility of MCC as a spheronization aid since source variation was removed as a confounding factor. It could possibly explain the inability of other proposed materials to serve as competent alternatives to MCC during extrusion-spheronization because these materials lack the microstructure that need to be composed of both large and small pores in order to function as an effective internal reservoir for water during wet massing and pellet production. This claim could be backed by the porosimetry data reported in another study (3) that investigated the usefulness of several size grades of cross-linked polyvinylpyrrolidone (crospovidone) to serve as competent spheronization aids. From the pore size distribution data

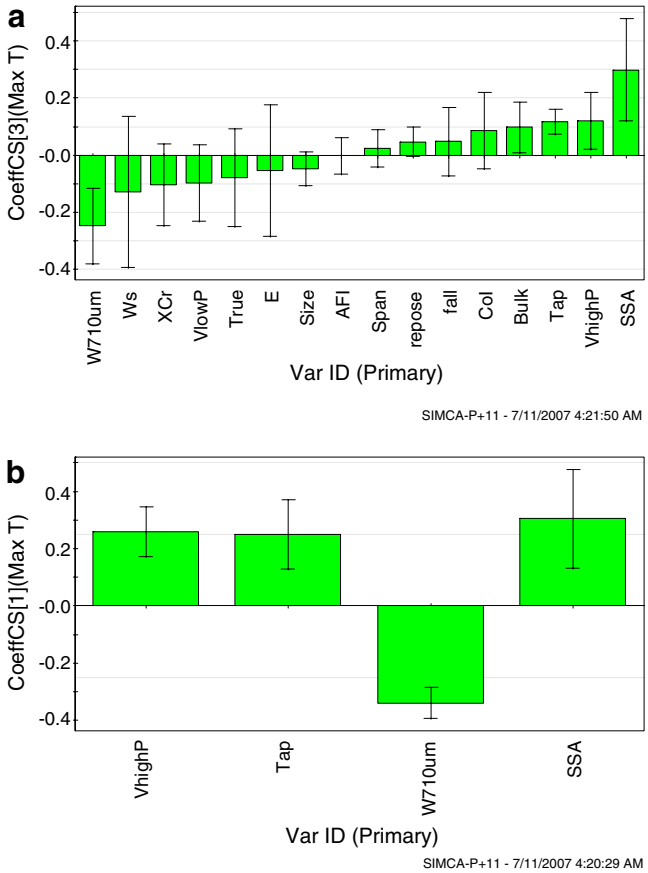

Fig. 7. PLS coefficients plot when all MCC physical properties were modeled (**a**) and only the significant variables were modeled (**b**). *E* denoted porosity while *Max T* denoted the $Torque_{max}$

reported in the study, Polyplasdone XL® was the only crospovidone grade that failed to facilitate extrusion-spheronization and it was also found not to have adequate pores lesser than 10 μm.

CONCLUSION

Size fractionated MCC grades from the same manufactured batch eliminated the major confounding factor of source variation to evaluate the significance of small pores in acting as a secondary reservoir to release a small but critical amount of water under stress. Together with knowledge gained from earlier studies, this finding provided preliminary evidence that the presence of small pores could play a role in MCC's unique functionality and efficiency as a spheronization aid. The extensive pre-formulation characterization of the fractionated MCC grades pointed to the significance of small pores in MCC's ability to control the rheological properties of wet masses. Additionally, the effects of MCC particle size and morphology on other physical characteristics were also aptly illustrated with this series of MCC grades.

ACKNOWLEDGEMENTS

The authors gratefully acknowledge the support and assistance of Mingtai Chemical Co, Taiwan, Republic of China for manufacturing the special MCC grades for this study. The Nagai Foundation, Tokyo, Japan is also acknowledged for providing the International Fellowship Research Grant (2006–2007) to Dr. Yang Lei. The authors also wish to acknowledge research funding support from the National University of Singapore Academic Research Fund (R-148-000-076-112).

REFERENCES

1. K. E. Fielden, J. M. Newton, P. O'Brien, and R. C. Rowe. Thermal studies on the interaction of water and microcrystalline cellulose. *J. Pharm. Pharmacol.* **40**:674–678 (1988).
2. P. Kleinebudde. The crystallite-gel-model for microcrystalline cellulose in wet-granulation, extrusion, and spheronization. *Pharm. Res.* **14**:804–809 (1997).
3. C. V. Liew, L. Gu, J. L. P. Soh, and P. W. S. Heng. Functionality of cross-linked polyvinylpyrrolidone as a spheronization aid: A promising alternative to microcrystalline cellulose. *Pharm. Res.* **22**:1387–1398 (2005).
4. P. W. S. Heng, and O. M. Y. Koo. A study of the effects of the physical characteristics of microcrystalline cellulose on performance in extrusion spheronization. *Pharm. Res.* **18**:480–487 (2001).
5. J. L. P. Soh, F. Chen, C. V. Liew, D. M. Shi, and P. W. S. Heng. A novel preformulation tool to group microcrystalline celluloses using artificial neural network and data clustering. *Pharm. Res.* **21**:2360–2368 (2004).
6. J. L. P. Soh, C. V. Liew, and P. W. S. Heng. Torque rheological parameters to predict pellet quality in extrusion–spheronization. *Int. J. Pharm.* **315**:99–109 (2006).
7. M. Whiteman, and R. J. Yarwood. Variations in the properties of microcrystalline cellulose from different sources. *Powder. Tech.* **54**:71–74 (1988).
8. F. Khan, and N. Pilpel. The effect of particle-size and moisture on the tensile-strength of microcrystalline cellulose powder. *Powder. Tech.* **48**:145–150 (1986).
9. M. Chatrath, J. N. Staniforth, I. Herbert, S. Y. Luk, and G. Richards. Source dependent polymorphism of microcrystalline cellulose. *J. Pharm Pharmacol.* **43**(Suppl.):7P (1991).
10. M. D. Parker, and R. C. Rowe. Source variation in the wet massing (granulation) of some microcrystalline celluloses. *Powder. Tech.* **65**:273–281 (1991).
11. P. H. Hermans, and A. Weidinger. On the determination of the crystalline fraction of polyethylenes from X-ray diffraction. *Makromol. Chem.* **44/46**:24–36 (1961).
12. R. L. Carr. Evaluating flow properties of solids. *Chem. Eng.* **72**:163–168 (1965).
13. H. H. Hausner. Friction conditions in a mass of metal powder. *Int. J. Powder. Metallurgy.* **3**:7–13 (1967).
14. J. L. P. Soh, C. V. Liew, and P. W. S. Heng. New indices to characterize powder flow based on their avalanching behavior. *Pharm. Dev. Technol.* **11**:93–102 (2006).
15. J. Soltys, Z. Lisowski, and J. Knapczyk. X-ray diffraction study of the crystallinity index and the structure of microcrystalline cellulose. *Acta. Pharm. Technol.* **30**:174–180 (1984).
16. J. H. Rose, J. Ferrante, and J. R. Smith. Universal binding energy curves for metals and bimetallic interfaces. *Phys. Rev. Lett.* **47**:675–678 (1981).
17. P. Colombo, P. Santi, F. Buttini, C. Sacchetti, G. Massimo, P. Russo, and R. Bettini. Particles and chimeral agglomerates for nasal drug administration. 14th International Symposium on Microencapsulation, Singapore, 2003, p. 6.
18. Y. S. L. Lee, R. Poynter, F. Podczeck, and J. M. Newton. Development of a dual approach to assess powder flow from avalanching behavior. *AAPS. PharmSciTech.* **1**:Article 21 (2000).
19. R. C. Rowe, and G. R. Sadeghnejad. The rheology of microcrystalline cellulose powder water mixes—Measurement using a mixer torque rheometer. *Int. J. Pharm.* **38**:227–229 (1987).
20. L. Eriksson, E. Johansson, N. Kettaneh-Wold, J. Trygg, C. Wikstrom, and S. Wold. Multi- and megavariate data analysis. Part I. Basic principles and applications, Umetrics Academy, Sweden, 2006.